LA-9042-PR

Progress Report

Betty B

C.3

Los Alamos National Laboratory is operated by the University of California for the United States Department of Energy under contract W-7405-ENG-36.

...nce Nuclear Safety and ...Fuels Program

May 1981

Los Alamos National Laboratory
Los Alamos, New Mexico 87545

The four most recent reports in this series, unclassified, are LA-8824-PR, LA-8865-PR, LA-8904-PR, and LA-8968-PR.

This work was supported by the US Department of Energy, Office of Coordination and Special Projects.

Edited by Betty Leffler
Photocomposition by Barbara J. Velarde
Assisted by Alice Creek

LA-9042-PR
Progress Report

UC-23
Issued: October 1981

Space Nuclear Safety and Fuels Program

May 1981

Compiled by

S. E. Bronisz

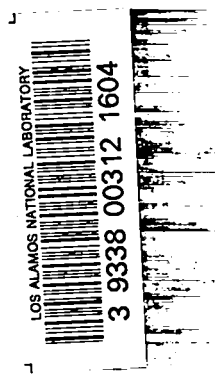

Los Alamos National Laboratory
Los Alamos, New Mexico 87545

SPACE NUCLEAR SAFETY AND FUELS PROGRAM
May 1981

Compiled by

S. E. Bronisz

ABSTRACT

This technical monthly report covers studies carried out by Los Alamos National Laboratory for the US Department of Energy, Office of Coordination and Special Projects, on the use of $^{238}PuO_2$ in radioisotopic power systems.

Most of the studies discussed here are of a continuing nature. Results and conclusions described may change as the work continues. Published reference to the results cited in this report should not be made without the explicit permission of the person in charge of the work.

I. GENERAL-PURPOSE HEAT SOURCE

The General-Purpose Heat Source (GPHS), a 250-W modular heat source fueled with ^{238}Pu, was developed by Los Alamos National Laboratory for the US Department of Energy. The final Los Alamos design was turned over to the Department in the Fall of 1979. Since that time, the Laboratory has been testing the design modifications introduced by the production agencies and has provided aid to the agencies during the start of production. In May the first Design Iteration Test (DIT-1) was completed, the proposed *in situ* reduction facility was analyzed, and investigations of iridium welding were carried out.

A. Impact Test (R. Zocher, C. Frantz, and F. Schonfeld)

DIT-1 was completed this month. For the test, a full General-Purpose Heat Source module was impacted on the broad face. All four fueled clads deformed similarly; none of them failed.

1. Test Objective. The DIT-1 impact was carried out on a full-sized GPHS module assembled at Los Alamos. This test used four $^{238}PuO_2$ fuel pellets for the first time, requiring significant changes in the handling procedures because of the additional heat.

a. Fuel. The fuel pellets used in the DIT-1 were fabricated by Savannah River Plant (SRP) as part of the normal production run. Because of the fear that the pellets might break apart during shipping, six were actually shipped. Each pellet was radiographed, removed from the shipping container, photographed, and measured.

All six pellets were cracked, but integral, as shown in Figs. 1-6. Their dimensions, weights, calculated densities, and neutron emmission rates are given in Table I. Two pellets were judged suitable only for emergency use:

Fig. 1. The ends of fuel pellet SRP-6 cracked in a crow's-foot pattern, and there was a defect at the lower knife-edge location. (1.5X)

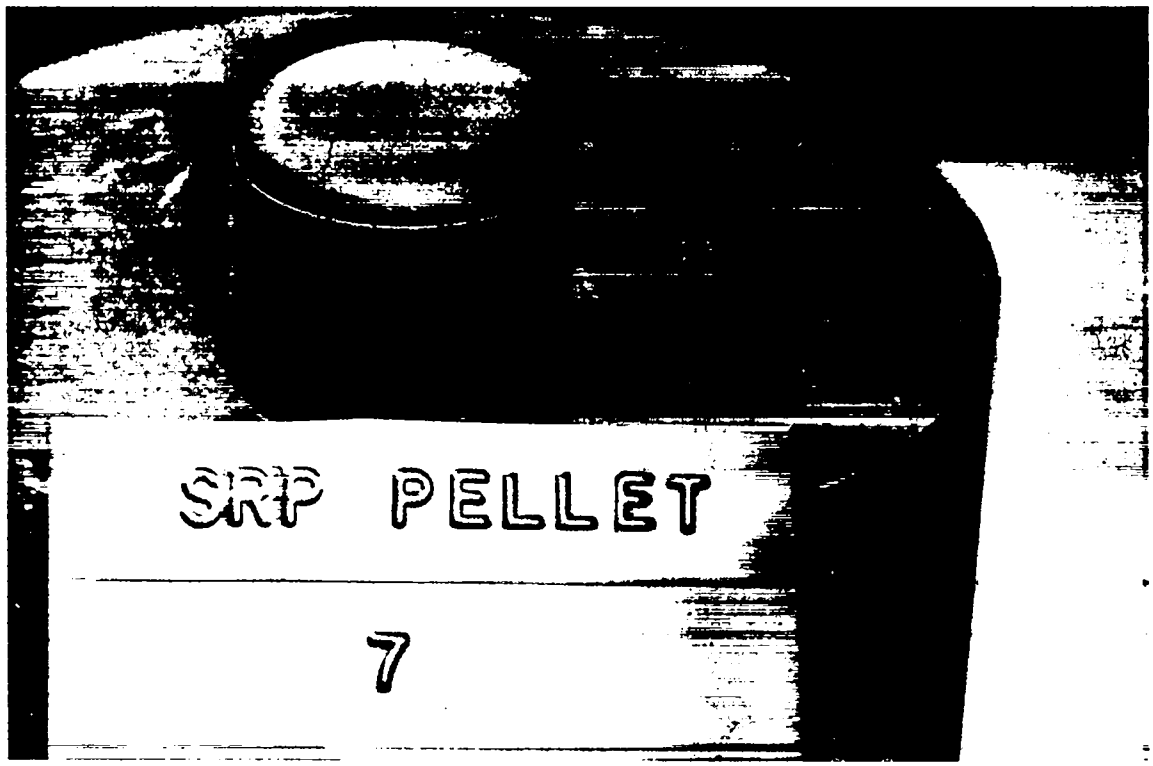

Fig. 2. The ends of fuel pellet SRP-7 contained several narrow cracks. (1.5X)

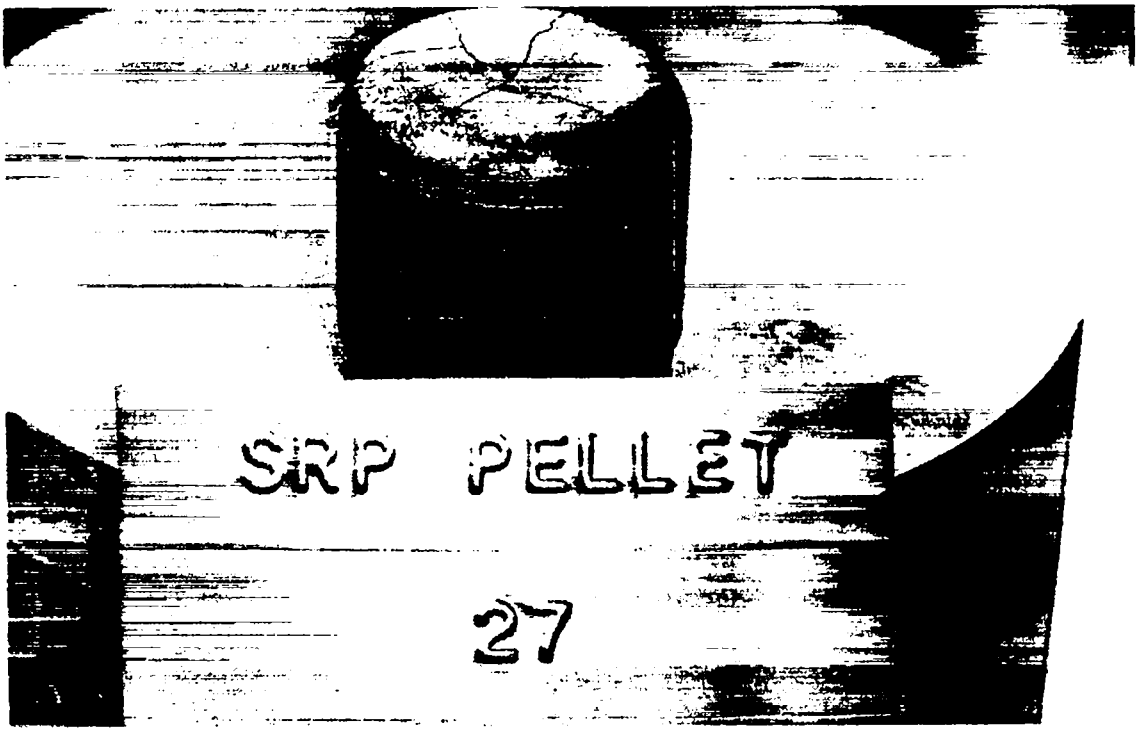

Fig. 3. The ends of fuel pellet SRP-27 were badly cracked and the radii were rough. (1.5X)

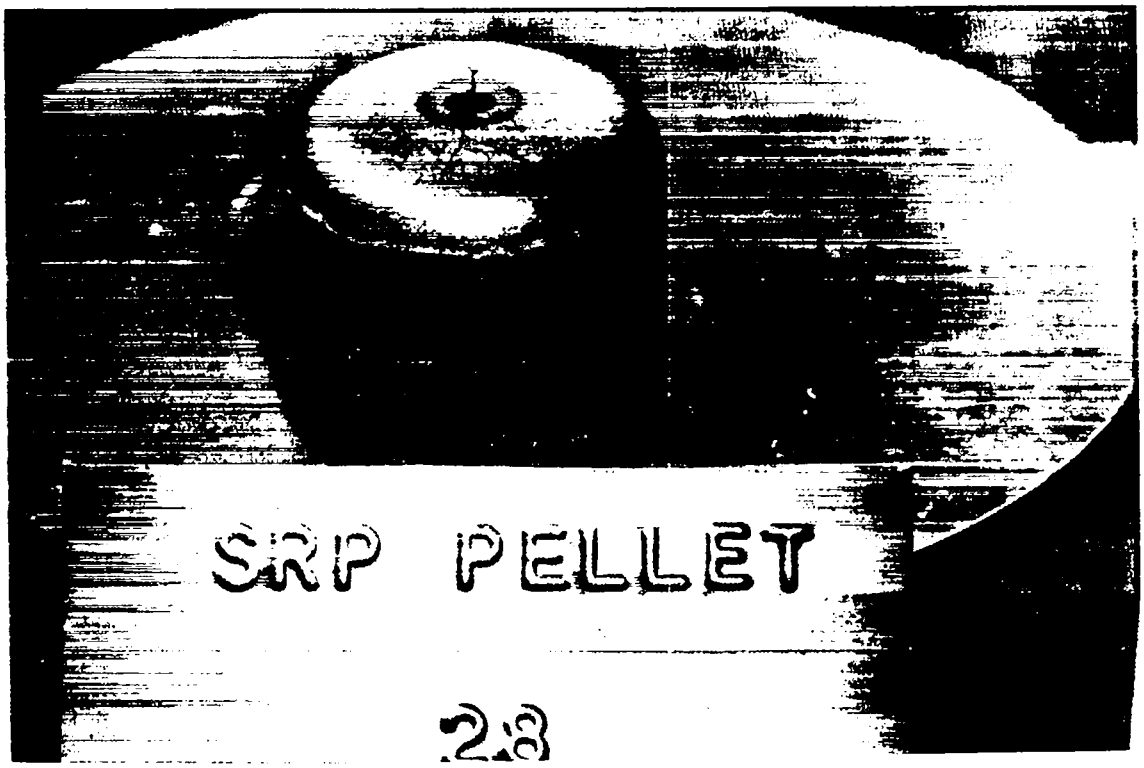

Fig. 4. The ends of fuel pellet SRP-28 were cracked, one end was stained, and there were multiple defects in the knife-edge location. (1.5X)

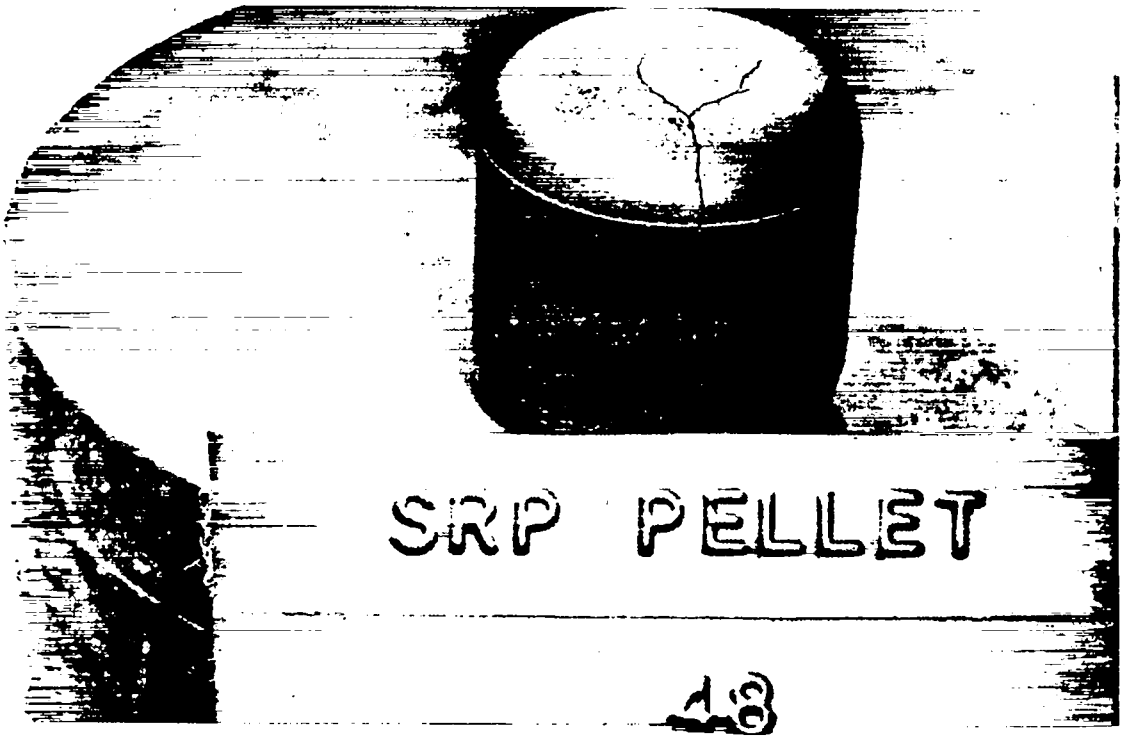

Fig. 5. The ends of fuel pellet SRP-48 were cracked in a crow's foot pattern. (1.5X)

Fig. 6. The ends of fuel pellet SRP-62 contained many cracks and the knife-edge regions were moderately defective. (1.5X)

TABLE I. Data for Sintered SRP Pellets

ID	Diam (mm)	Length (mm)	Weight (g)	Density (% TD)	Neutron[a] Emission Rate (n/s-g ^{238}Pu)
SRP 6	27.61	27.66	149.32	83.6	5 833
SRP 7	27.61	27.69	149.54	83.6	6 639
SRP27	27.69	27.74	149.74	83.1	5 915
SRP28	27.74	27.81	149.82	82.6	
SRP48	27.71	27.84	149.07	82.3	5 905
SRP62	27.33	27.33	147.47	85.3	

[a]Measured at Los Alamos after the capsules were welded.

SRP-28, because of the spot visible on its upper face in Fig. 4, and SRP-62, because of its significantly smaller dimensions and higher density.

b. Capsules. Six iridium clad-vent sets were supplied by Mound Facility (MF) after they had been annealed for 20 h at 1500°C. Two of these were flight quality, two were for engineering use only, and two were for example-weld use only. The components of the clad-vent sets are identified in Table II.

c. Graphite. The graphite components were described last month.[1] Briefly, the aeroshell and impact shells were machined to specification at Los Alamos. The aeroshell thickness was uniformly reduced by 1.25 mm, and the corners of the impact shells were coated with 0.5-mm-thick layers of pyrolytic graphite by Pfizer, Inc. The insulation was engineering-use-only material supplied by Oak Ridge National Laboratory (ORNL).

2. **Encapsulation.** The capsules were loaded with the fuel pellets and welded in the order shown in Table II. The scheduled example-weld assembly, IRG-105, was welded over Los Alamos pellet GP-58. The capsule was cut open along a circumference displaced from the weld. The weld was examined at a magnification of 7X. No cracks were found and penetration was complete at all points, so the next four capsules were welded for use in the impact test. Finally, capsule IRG-106 was welded over Los Alamos pellet GP-58. The iridium cups that made up IRG-106 were poorly matched, having a 0.15-mm diametral difference. They had been relegated to the backup role because of this mismatch. Capsule IRG-106 was opened, and the fuel pellet was removed. Both IRG-106 and IRG-105 were submitted for metallographic examinations. A 1.7-mm-long crack was found in the weld overlap region of IRG-106.

The four fueled clads to be used in the impact test were decontaminated to zero swipe and transferred to the metallography facility, where they were inspected.

3. **Weld Inspection.** Two preconditions were placed on the use of fueled clads IRG-101 through IRG-104 in the DIT-1 impact: the weld exteriors had to be of good appearance, and the example weld on IRG-105 had to be closely similar to that of the previously impacted IRG-90.

The welds on the four test capsules were of good appearance. An example, the weld on IRG-104, is shown in Fig. 7. In addition to the weld examination, each capsule was examined for circumferential uniformity by rotating it on a sighting square made of graphite. All four capsules had similar tapered-barrel shapes, because they were made from slightly tapered cups. IRG-101 displayed a uniform amount of bulging around its circumference. Its 0.25-mm bulge was defined as the standard. IRG-102 had a region about 120° from the weld overlap that bulged 0.37 mm. The bulge on IRG-103 was a relatively uniform 0.20-0.25 mm except for the 30° before the overlap, where it was only 0.12 mm. The bulge of IRG-104 was irregular, ranging from 0 to 0.37 mm around the circumference. We did not perform a preweld inspection of the cups, so we don't know the source of the variations.

A cross section of the weld on example-weld capsule IRG-105 is shown in Fig. 8 along with a similar section of capsule IRG-90. The welds are very similar, as required.

TABLE II. Encapsulation Details for DIT-1 Fueled Clads

Assembly No.	Iridium Cup Vent	Iridium Cup Shield	Quality[a]	Fuel Pellet[b]	Use
IRG-105	L240-4	L260-5	EWO	GP-58	example weld
IRG-103	L307-1	L243-4	EUO	GPHS-6	impact
IRG-104	LR308-2	L241-3	EUO	GPHS-7	impact
IRG-101	LR302-8	LR269-3	FQ	GPHS-27	impact
IRG-102	LR305-3	LR238-4	FQ	GPHS-48	impact
IRG-106	L263-8	LR297-5	EWO	GP-58	example weld

[a]EWO = example weld only, EUO = engineering use only, and FQ = flight quality.
[b]GP = Los Alamos manufacture, and GPHS = Savannah River Plant manufacture.

Fig. 7. The weld of IRG-104 was typical of those on the four DIT-1 fueled clads.

4. Weld Annealing. The four capsules to be impacted, IRG-101 through IRG-104, were annealed for 100 h at 1306°C to condition the welds. ORNL recommends this heat treatment, because it simulates the expected temperature history of the flight heat sources and because it leaves the welds more ductile.

The weld anneals were carried out in vacuum resistance furnaces with the fueled clads in impact shells, which were held in outgassed ATJ graphite containers. Before assembly, the vent covers on the capsules were removed. The capsules were placed in the impact shells with the weld overlap areas opposite the intended impact surface. The clad temperature of the top capsule in each impact shell was sensed directly on-axis with a Pt-Rh thermocouple, which penetrated the ATJ cover and the impact shell closure. The graphite components used in the weld annealing are shown in Fig. 9.

5. Impact Test. After the weld anneal, the fueled impact shells were transferred to an inert-atmosphere box, where they were assembled into a module along with new, outgassed insulators and the previously prepared and outgassed aeroshell. The module was then placed on the sabot with a single thermocouple in contact with IRG-102, one of the flight-quality clads. The transfer container, described last month,[1] was assembled and filled with helium, and the cooling fan was started. The next morning the capsule IRG-102 had reached an equilibrium temperature of 318°C. The laboratory air was at 25.6°C. The transport container was cooled with dry ice and shipped to the gun site. Immediately before insertion, IRG-102 was at 309°C. Insertion required 5 min from the time the seal on the transport container was broken to the time evacuation of the gun barrel was started.

Immediately after the evacuation was started, the temperature of IRG-102 was 350°C. Within an hour, it

(a)

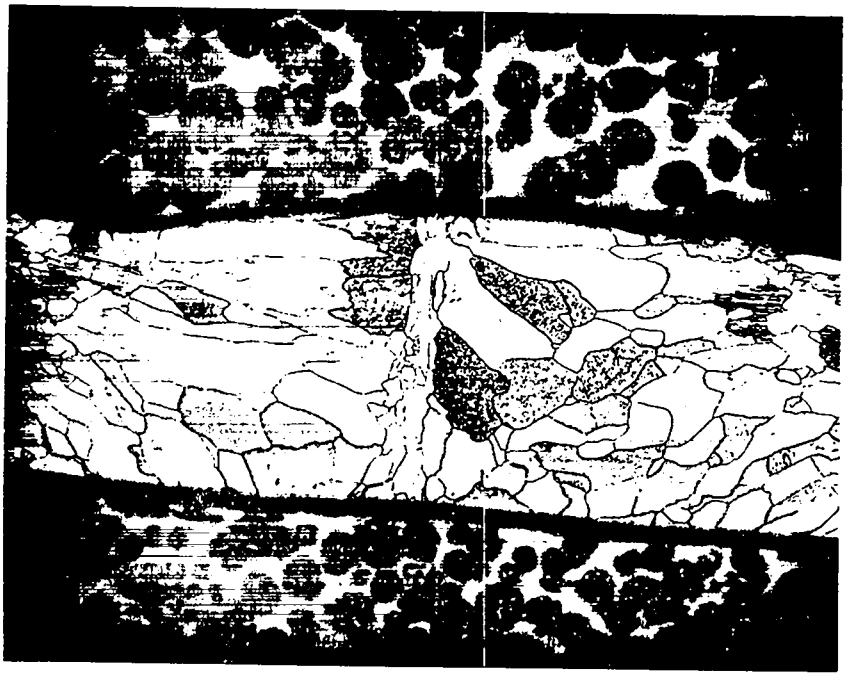

(b)

Fig. 8. The welds of of capsules IRG-105 (a) and IRG-90 (b) had very similar microstructures. (50X)

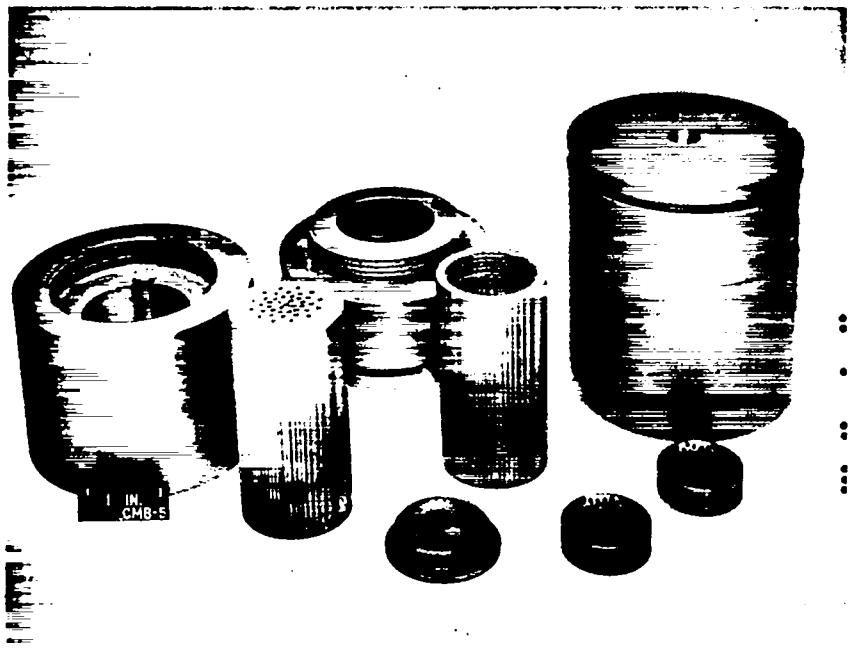

Fig. 9. The fueled clads were annealed for 100 h at 1306°C in impact shells held in ATJ graphite containers.

had increased to 485°C. The intended impact temperature of 930°C was reached after an additional 6900 s, and the module was impacted at 57.0 mps. The sealed inner catch tube was recovered and transferred to the disassembly area in the CMR Building.

No plutonium was detected when the inspection port was opened, so the catch tube cover was removed, revealing the impacted module. The impact face of the aeroshell had been broken, and the two impact shells, glowing with a temperature of 700-750°C, could be seen. On exposure to freely available air, the impact shells started to burn, so they were broken out of the remains of the aeroshell and put in a glove box to cool.

The remains of the aeroshell and insulators are shown in Fig. 10. Before removal of the impact shells, the impact face of the aeroshell was broken into uneven slabs 6-12 mm wide and 24-50 mm long. The aeroshell had cracked on the sides parallel to the impact shell axes, and its threaded closure had come out.

The recovered impact shells were quite similar in appearance, as can be seen in Fig. 11. The impact side was battered and cracked for most of its length, and the end caps were displaced and loose. The impact shells were bowed nearly 1 mm toward the unsupported center.

The four fueled clads were removed from the impact shells with little difficulty. None had failed and all were remarkably similar in appearance, as shown in Fig. 12. Each was flattened on the impact side. The deformation was asymmetric, with each capsule showing the same kind of protrusion toward the internal window of the aeroshell. The measured strains for the four fueled clads used in DIT-1 are listed in Table III.

This initial test in the most probable orientation and with a moderate iridium grain size was a success in that none of the capsules failed and no fuel was released. The capsules will be sectioned, and they and the fuel will be examined in June.

B. Iridium Welding (F. W. Schonfeld)

Since the iridium welding procedure for GPHS capsules was worked out in 1979, we have seen no weld failures on impact as long as that procedure was followed. Because the welds did not fail, we paid them scant attention. This attitude was reinforced by the knowledge that welding was to be performed at Los Alamos only until the SRP welding facility was certified for production.

Unfortunately, SRP has been plagued with weld cracking in the overlap region during their start-up operations. The typical crack they observed is shown in Fig. 13. They supplied the sample, SR-28-D, so that we could know what cracks look like. We had never noticed a crack like that shown in the figure in an unimpacted capsule, but we reviewed our metallographic results and reexamined those capsules still available. The results are listed in Table IV.

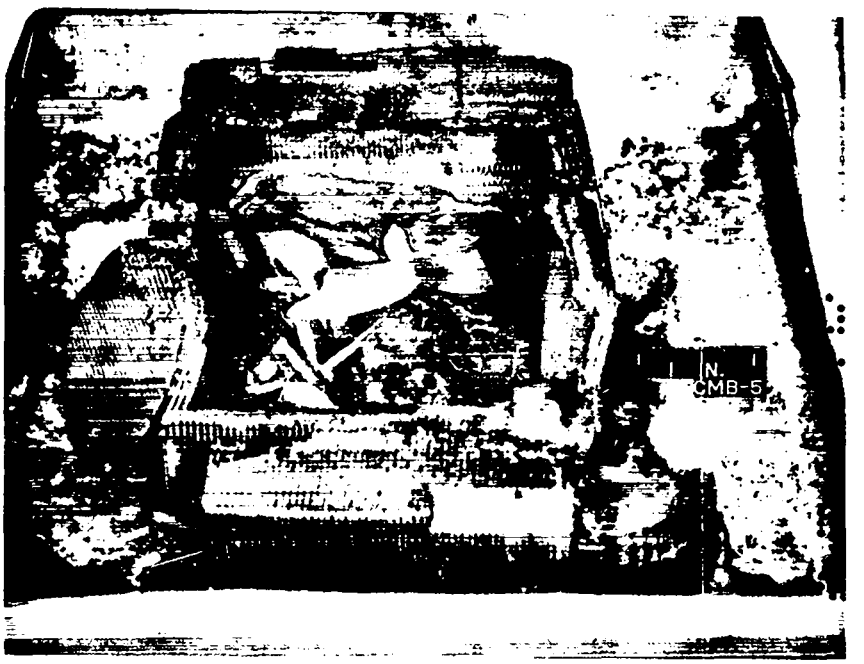

Fig. 10. The aeroshell and insulators were broken by the impact. The separation of the fragments occurred when the impact shells were removed.

Not all of the capsules welded at Los Alamos could be examined. Of those that could, four were cracked in the weld overlap region. All four had been impacted before examination, and it is not possible to determine unequivocally when the cracks formed.

The SRP weld, SR-28-D, and two Los Alamos welds of older, developmental iridium cups, IRG-36 and IRG-39, were sectioned for Auger analysis to determine if there were any gross differences between the current iridium and the older material on which most of the Los Alamos welds were made. Four samples were taken from each capsule: one from each cup wall in a region unaffected by the weld, one through the weld in the single-pass region, and one through the weld overlap.

The Auger analysis results are listed in Table V. The samples of the walls and the welds show the usual scatter in thorium/iridium for all samples examined, as do the fresh fractures in the overlap samples. The exposed surface of the weld crack in sample SR-28-D had relatively large amounts of silicon, carbon, and oxygen and a smaller amount of sulfur. Sputtering removed the first three and reduced the sulfur level. Except for the sulfur, these elements probably were contaminants introduced after the crack formed and are unrelated to the causes of the crack.

Perhaps the only important conclusion to be drawn from these data is that enrichment of thorium in the weld metal grain boundaries is very modest, at best, and provides no support for the thorium-iridium eutectic, hot-short postulate. The generally brittle behavior of grain boundaries in the alloy is well documented. We have observed small grain-boundary cracks at weld edges that extend into both weld and wall; therefore, the characteristics of the wall and weld grain boundaries must be similar. These data also suggest that the current iridium alloy is not greatly different in composition from other lots.

If one accepts these statements, a logical next step might be to postulate that the alloy is basically a material of poor weldability and that microstructure and thermal stress are critical factors. In the early stages of welding, the metal is relatively free to expand and contract (despite the tack welds), but it becomes more constrained as the welding progresses. The maximum thermal stress would occur immediately after the closure was effected. Consider the physical state of the metal at this time. There is a mixed-phased weld, a solid portion of the first-pass weld metal that has not remelted, but that is overlaid by a pool of remelted metal. Because of the rigidity of the closed capsule, the solid layer cannot

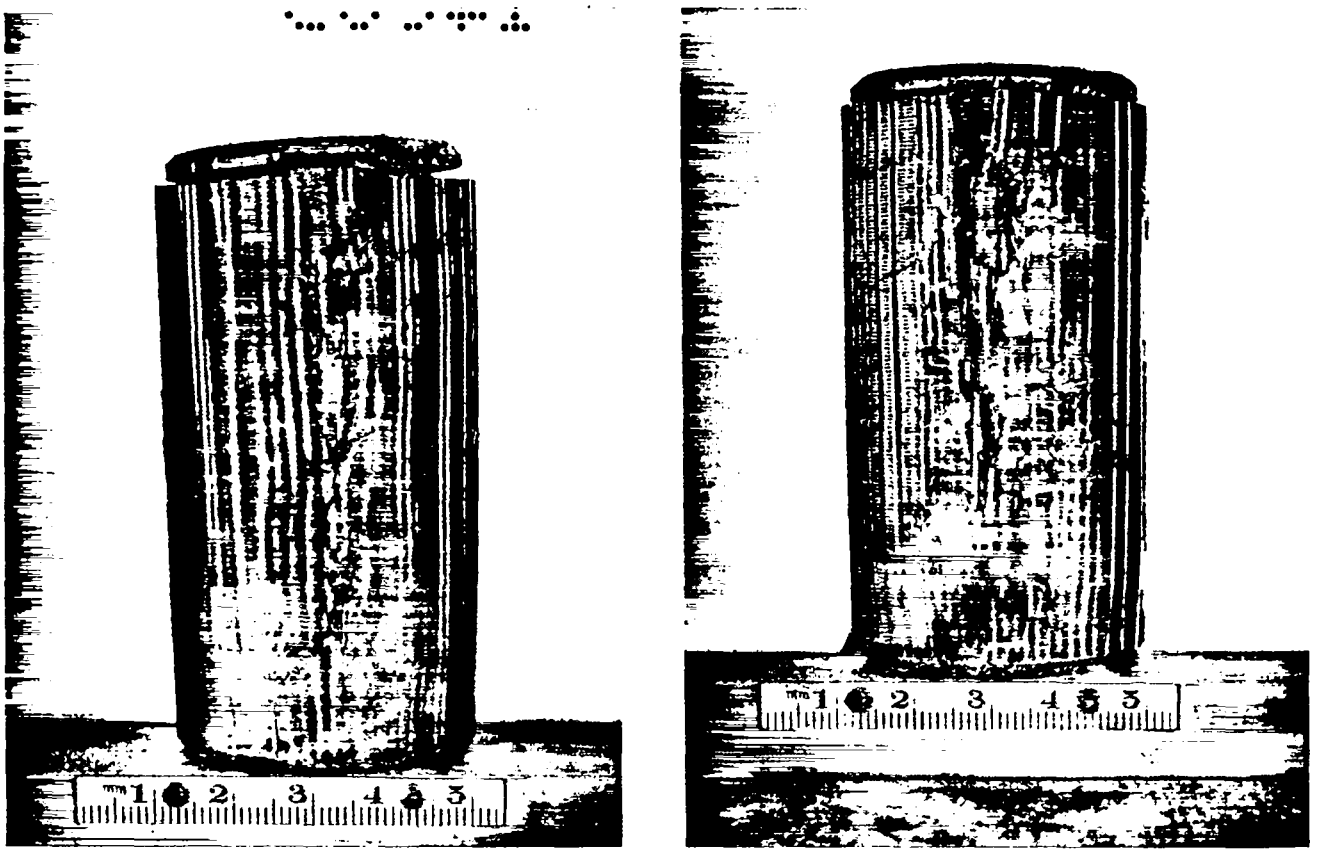

(a) (b)

Fig. 11. The two impact shells appeared quite similar after the DIT-1 impact; (a) IRG-101 and IRG-102; (b) IRG-103 and IRG-104.

expand freely during heat-up and so must plastically deform and upset slightly. If the upset portion of the overlap is thin, it may be unable to sustain the contraction stresses during cooling and may crack. Obviously, to minimize the extent of this zone the power ramp must be steep, and the total length of the overlap should be held to a minimum.

Thermal stresses can be minimized, but they cannot be eliminated. In a given situation the grain size and orientation may determine whether a weld will crack. In general, two factors will govern the grain size of the weld metal: the grain size of the parent metal and the cooling rate through the solidification range. The welder ordinarily has no control over the grain size of the parts he is to assemble; cooling rate is his only available control. It would seem that effective and symmetrical chill-blocks should be provided—a conclusion that is supported by the extensive experience in successfully welding Multi-hundred Watt (MHW) spheres at MF and SRP.

The extent of possible effects of grain orientation on weld cracking is not known. There are two possibilities to be considered: first, that grain orientation can affect the tendency to crack, and, second, that location of the overlap on the capsule circumference can influence the cracking tendency. We are examining both.

When weldments in the DOP-26 iridium alloy are etched with the NaCl-saturated NaOH reagent introduced by SRP, the dendritic patterns of tungsten segregation are revealed. An example of the patterns in sample SR-28-D is shown in Fig. 14. That this segregation is of tungsten is demonstrated by the similar structure present in the arc-melted Ir-5 wt% W sample shown in Fig. 15. This etchant also produces well-defined etch pits in grains with {111} faces exposed, as shown in Fig. 16. This orientation sensitivity may be useful in the study of orientation effects.

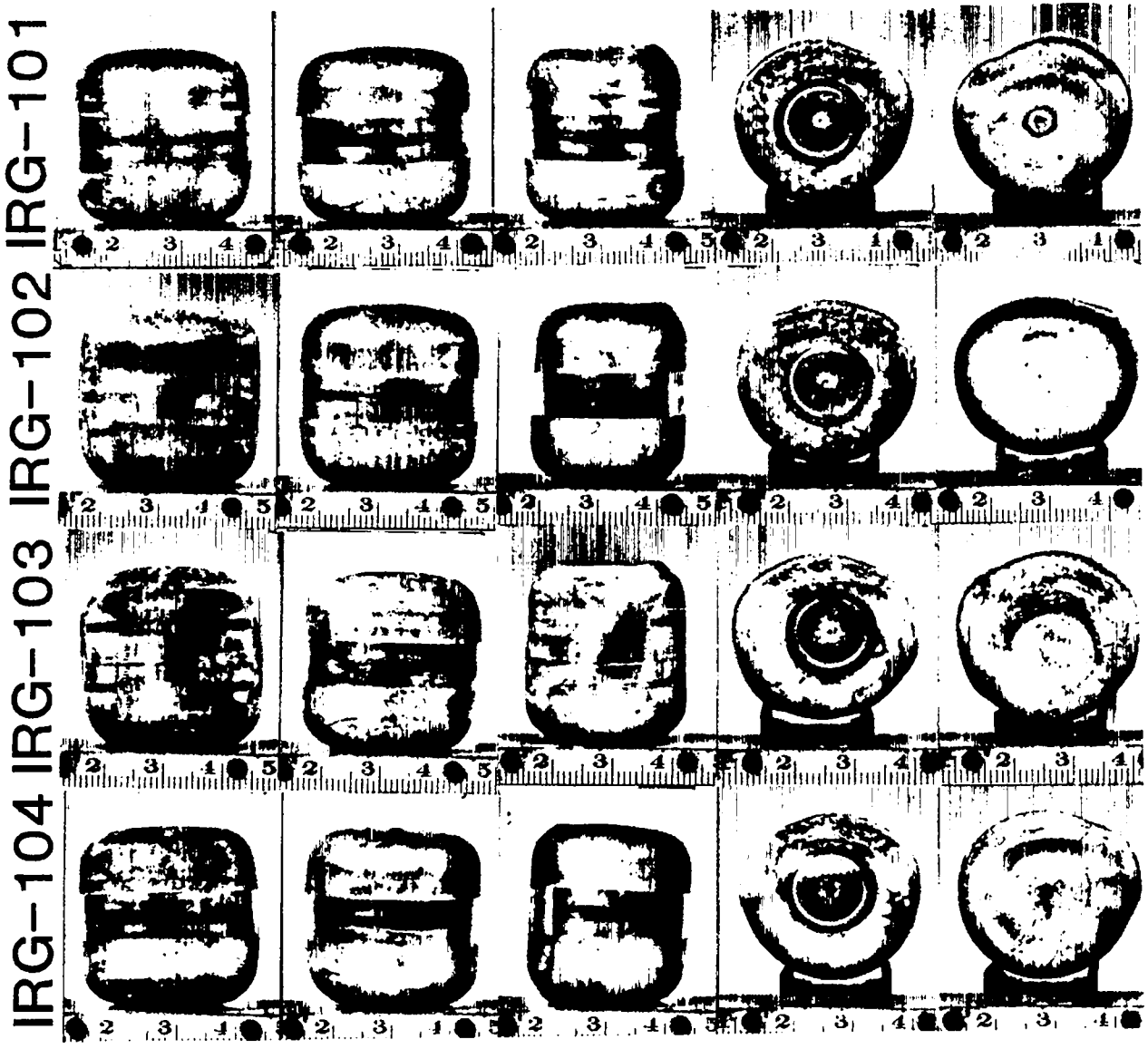

Fig. 12. All four fueled clads in the DIT-1 impact showed similar deformations.

TABLE III. Measured Impact Strains on DIT-1 Fueled Clads

Strain Type/ Location	Engineering Strain (%)							
Capsule	101		102		103		104	
Diametral								
Top cylinder	5.5	-4.8	5.6	-6.5	6.7	-8.0	6.3	-4.6
Weld	6.5	-4.2	7.3	-7.1	7.0	-5.7	6.3	-3.6
Bottom cylinder	4.8	-7.2	6.2	-7.8	5.5	-5.0	7.0	-4.1
Diagonal								
Wide face	1.1	1.3	0.9	1.4	0.95	1.6	1.5	1.6
Thickness	-2.7	-2.7	-4.0	-0.8	-4.7	-2.6	-3.5	-2.3
Length								
Max	2.9		5.7		3.0		5.0	
Min	2.4		5.0		2.0		3.9	

C. In-Module Fuel Reduction (D. Peterson and J. Starzynski)

The proposed treatment of GPHS modules with CO was more extensively analyzed this month. A computer program was written to solve for the final CO pressure and the O/Pu ratio in the fuel. The input variables were the initial CO pressure, the initial fuel stoichiometry, the graphite and fuel temperatures, the system void volume, and the fuel mass. The oxygen potentials of selected fuel stoichiometries were based on Markin and Rand's[2] measurements as reviewed by Ackermann *et al.*[3]

In a closed volume, the CO pressure increases as the fuel is reduced. The fuel reduction stops when the oxygen potentials of the fuel and CO are equivalent. In the proposed system, evacuation and refilling of the treatment chamber would constitute a second treatment cycle that would result in a further lowering of the fuel stoichiometry.

The graphite and fuel temperatures during the CO treatment must be known if the extent of the fuel reduction is to be calculated accurately. We assumed three graphite and fuel temperature conditions: 1000 and 1200°C, 1250 and 1461°C, and 1250 and 1540°C. They correspond to the proposed conditions in Ar-4 wt% CO, the average fuel temperature in vacuum, and the centerline fuel temperature in vacuum, respectively.

The final CO pressures and O/Pu ratios attained in each of five cycles for the three temperature combinations are shown in Table VI. The 3 cases treated are for 2 modules in a closed can, 2 modules in a can open to the manifold, and 32 modules in 16 cans open to the manifold. The results in each case show that copious quantities of CO form as the fuel is reduced. The actual pressures and reductions for the two vacuum cases would be less than indicated, of course, because the CO formed would spoil the vacuum and the temperatures would fall. The calculated results show that the addition of a ballast volume to the manifold would speed up the fuel reduction.

The stoichiometries calculated in this analysis remain above those that would lead to reaction with the iridium cladding. Under normal conditions the reaction would be self-limiting, as explained above. If, however, the system were to leak so that the CO did not build up, the reduction would continue to even lower stoichiometries.

Fig. 13. Savannah River Plant iridium capsule SR-23-D was cracked in the weld overlap region. (8X)

TABLE IV. Crack Survey Results for Iridium Capsules Welded at Los Alamos and Examined for Overlap Cracks

Capsule No.	Impacted?	Overlap Crack?	Comments
IRG-15	Yes	No	
IRG-19	Yes	No	
IRG-20	Yes	No	
IRG-27	Yes	No	
IRG-28	Yes	No	
IRG-29	Yes	No	
IRG-30	Yes	No	Poor centerline structure
IRG-36	No	No	
IRG-37	Yes	Yes	Fine grain-boundary crack
IRG-39	No	No	
IRG-42	Yes	No	
IRG-43	Yes	No	
IRG-57	Yes	Yes	Fine crack, seen with SEM
IRG-87	Yes	No	
IRG-88	Yes	Yes	Impact induced
IRG-101	Yes	No	
IRG-102	Yes	No	
IRG-103	Yes	No	
IRG-104	Yes	No	
IRG-105	No	No	
IRG-106	No	Yes	

TABLE V. Auger Analysis Results for Three Welded Iridium Capsules

Spec. No.	Description	Location	Th_{65}/Ir_{229}	S_{150}/Ir_{229}	Other/Ir_{229}
SR-28-D-1	wall	inside	0.23	-----	-----
		center	0.25-0.31	-----	-----
		outside	0.17		
SR-28-D-2	wall	inside	0.50	-----	-----
		center	0.70	-----	-----
		outside	0.33		
SR-28-D-3	weld	inside	0.30-0.82	-----	-----
		center	0.50-0.56	-----	-----
		outside	0.07-0.39	-----	-----
SR-28-D-4	overlap (fresh)	inside	0.11-0.83	-----	-----
		center	0.58-0.85	-----	-----
		outside	0.36	-----	-----
	weld crack	inside	0.11	0.29	Si_{92}: 0.33-11.6 C_{270}: 3.6-17.3 O_{510}: 7.3-50.4
		center	tr-0.63		
		outside	tr.		
	weld crack (sputtered)	inside	0.06	0.01	
		outside	tr.	0.02	
IRG-36-A-1	wall	inside	0.70		
		center	0.78		
		outside	0.31		
IRG-36-A-2	wall	not suitable for analysis			
IRG-36-A-3	weld	not suitable for analysis			
IRG-36-A-4	overlap	inside	0.35		
		center	0.44		
		outside	0.0	0.02	
IRG-39-A-1	wall	inside	0.45-0.75		
		center	0.72		
		outside	0.16		
IRG-39-A-1	wall	inside	0.30-0.61		
		center	0.74		
		outside	0.40		
IRG-39-A-3	weld	inside	0.47		
		center	0.47		
		outside	0.42		
IRG-39-A-4	overlap	inside	0.51-0.72		
		center	0.66		
		outside	0.46		

II. SYSTEMS SUPPORT (D. Pavone)

The MHW fuel sphere assembly MHFT-75, a production surveillance sample, was aged 30 days, was subjected to the standard 1500°C reentry-heating temperature pulse, and was impacted at 1430°C and 81 mps.

The impact can deformed symmetrically, and the impact occurred with the cap of the graphite impact shell oriented 180° from the initial impact point. The impact shell was split and delaminated.

Photographs of the impacted iridium-clad fuel sphere are shown in Fig. 17. The weld plane of the iridium shell was oriented at about 45° to the face of the polished granite target. No hoop failures, fuel push-through penetrations, or fingerprint cracks were observed. The height strain was -26.0%, and the diametral strain varied from +6.6 to +8.3%.

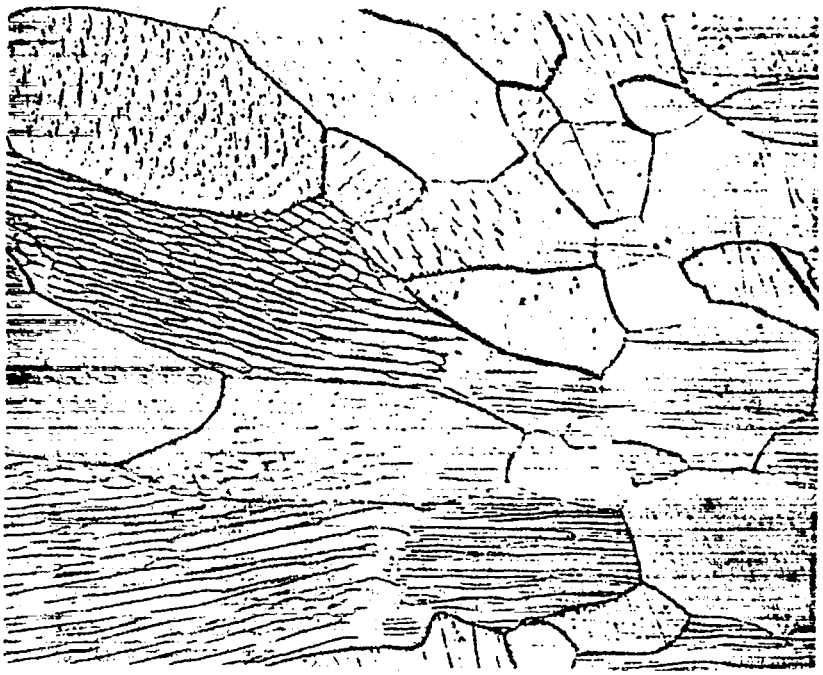

Fig. 14. Microstructure of weld boundary of specimen SR-28-D. The microsegregation of tungsten is revealed in both the as-rolled grains and the weld pool. The strong epitaxial growth of the weld metal on the unmelted grains is also evident. (250X)

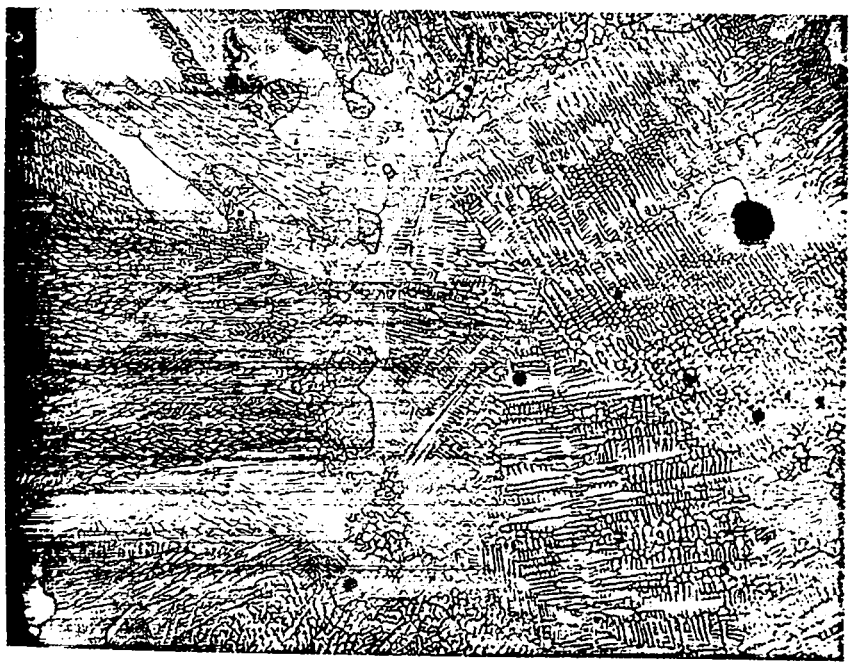

Fig. 15. The dendritic segregation of tungsten in an arc-melted sample of Ir-5% W was revealed by the NaCl-saturated NaOH solution. (40X)

The weld band was intact and there was no visual evidence of iridium transport. Both vent assemblies were open when tested with helium at 138 kPa.

Radiochemical analysis of the ash obtained from combustion of the recovered impact shell debris indicated a total plutonium content of 164 μg and a phosphorous content equivalent to 63 ppm. The plutonium content is higher than that usually observed.

A metallographic cross section including the weld and sections of both hemispheres of the iridium shell showed the microstructure of the weld bead to be excellent, as shown in Fig. 18, and the grain size of the hemispheres to be 8.9 and 9.1 grains/thickness. A thin layer of iridium grains, partially detached from the surface, was observed on the interior of the iridium shell.

Fig. 16. The NaCl-saturated NaOH etchant produced etch pits on a {111} grain in SR-28-D. (250X)

TABLE VI. Fuel Stoichiometry and CO Pressure after CO Treatment

	Conditions[a]	Cycle	Temperature, Graphite and Fuel (°C) 1000 and 1200 P_{co}(atm)	O/Pu	1250 and 1461 P_{co}(atm)	O/Pu	1250 and 1540 P_{co}(atm)	O/Pu
1.	Two modules closed can Vol. 2070 cm^3 PuO_2: 1249 g	1	2.0	1.992	21.7	1.922	24.5	1.912
		2	1.5	1.985	7.4	1.895	7.7	1.884
		3	1.3	1.980	4.2	1.880	4.3	1.869
		4	1.1	1.975	2.9	1.870	2.9	1.858
		5	0.92	1.972	2.2	1.863	2.2	1.851
2.	Two modules open to manifold Vol. 7254 cm^3 PuO_2: 1240 g	1	1.3	1.981	8.1	1.898	8.9	1.888
		2	0.83	1.969	2.5	1.866	2.6	1.855
		3	0.60	1.960	1.4	1.850	1.4	1.838
		4	0.48	1.953	0.94	1.838	0.95	1.826
		5	0.39	1.948	0.71	1.830	0.72	1.818
3.	32 modules, 16 cans, open to manifold, Vol. 38 438 cm^3 PuO_2: 18 740 g	1	1.9	1.990	19.4	1.919	21.8	1.909
		2	1.5	1.984	6.5	1.892	6.8	1.881
		3	1.2	1.978	3.7	1.877	3.8	1.865
		4	0.98	1.973	2.5	1.867	2.6	1.855
		5	0.84	1.969	1.9	1.859	1.9	1.847

[a] Initial O/Pu = 2.000, initial P_{CO} = 0.04 atm.

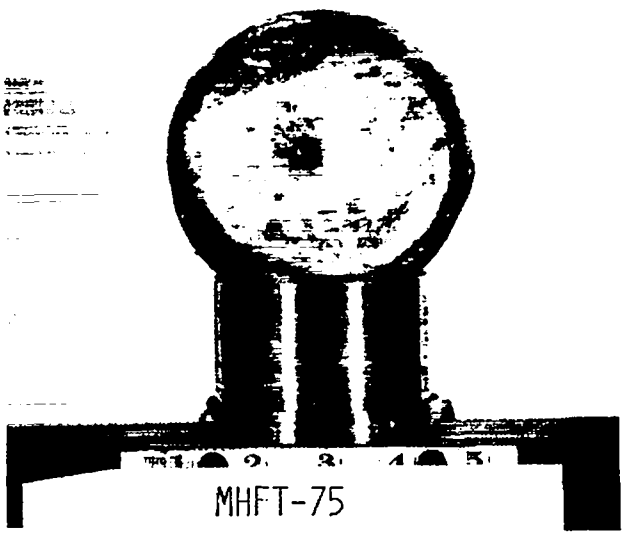

(a)

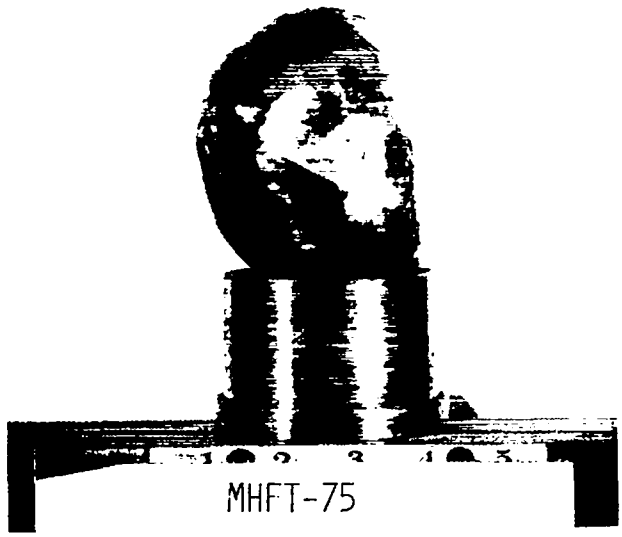

(b)

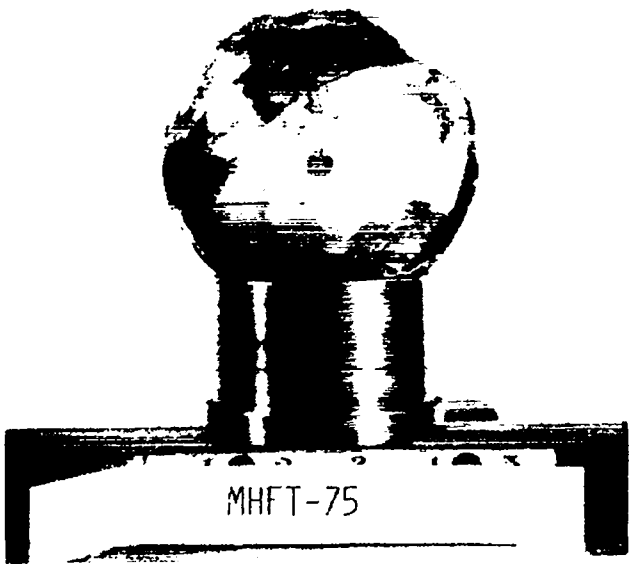

(c)

Fig. 17. Photographs of the impact iridium shell of MHFT-75. There were no failures. (a) face, (b) profile view, and (c) back side. (~1X)

Metallographic examination of cross sections of the vent assemblies revealed heavy deposition of nonmetallic material in the interstices of the iridium filter element, including a constituent having a eutectic structure, as shown in Fig. 19, and nonmetallic material deposited on the wall of the vent hole, as shown in Fig. 20.

The constituents of the nonmetallic deposits in the vent structure as determined by electron microprobe analysis were as follows.

Major phase: plutonium, iron, silicon, magnesium, calcium, manganese, tungsten, titanum, and oxygen.

Minor phase 1: plutonium and oxygen.

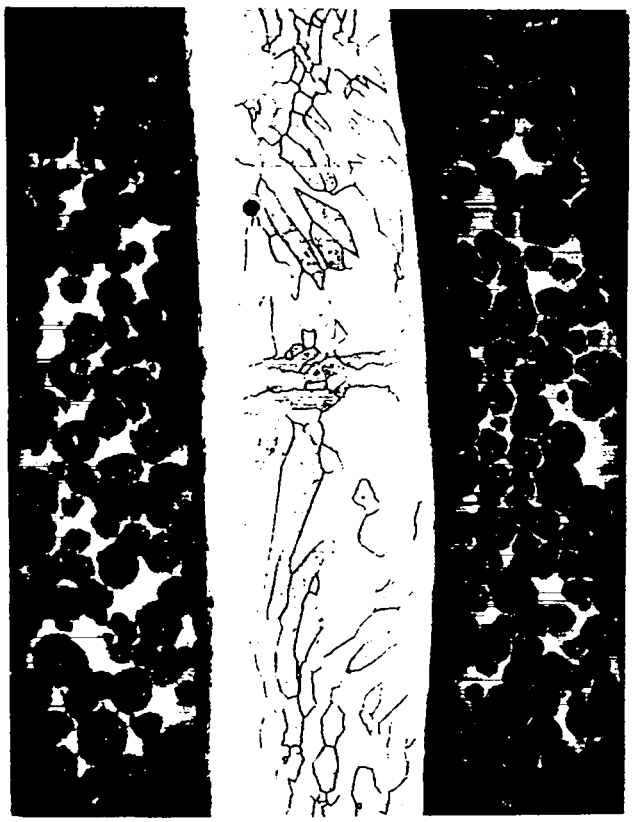

Fig. 18. Microstructure of the weld bead of MHW-FSA MHFT-75. (40X)

Minor phase 2: plutonium, iron, silicon, calcium, magnesium, tungsten, and oxygen.

Eutectic: plutonium, iron, silicon, calcium, magnesium, tungsten, and oxygen.

Both phases deposited in the vent hole contained plutonium and oxygen with the light-gray phase showing the higher concentration of plutonium. The appearance of plutonia at this location correlates with the higher amounts of plutonium found in the impact-shell debris.

Spectrographic analysis of a sample of the impacted plutonia sphere showed the major impurities to be (in ppm): magnesium—50, aluminum—65, silicon—110, chromium—50, iron—170, calcium—150, and tantalum—250. These impurity levels are within the specification; they contrast with MHFT-74, in which similar vent deposits were seen, but high levels of calcium, magnesium, and silicon were observed in the plutonia. Chemical analysis of the plutonia revealed a phosphorous content of 10 ppm. The pretest γ-scan had indicated <20 ppm of phosphorus.

Metallographic examination of the plutonia did not reveal the presence of significant quantities of grain-boundary helium bubbles. The microstructure of samples from the surface and the core are shown in Fig. 21. It is unusual to observe the marked grain size difference between the surface and core regions illustrated in these photomicrographs.

The results of the 12 Galileo-related MHW impact tests are listed in Table VII. Three samples remain to be tested.

III. LIGHT-WEIGHT RADIOISOTOPE HEATER UNIT

A. Production (R. A. Kent)

1. Fueled Units. Fifteen ^{238}PuO pellets were encapsulated in Pt-30 wt% Rh hardware, 2 of them in developmental capsules and 13 in prime capsules. The pellet and capsule identification numbers and dimensions, together with the weld box atmospheres, are summarized in Table VIII. Seven of the prime capsules will be shipped for the Galileo mission, together with the

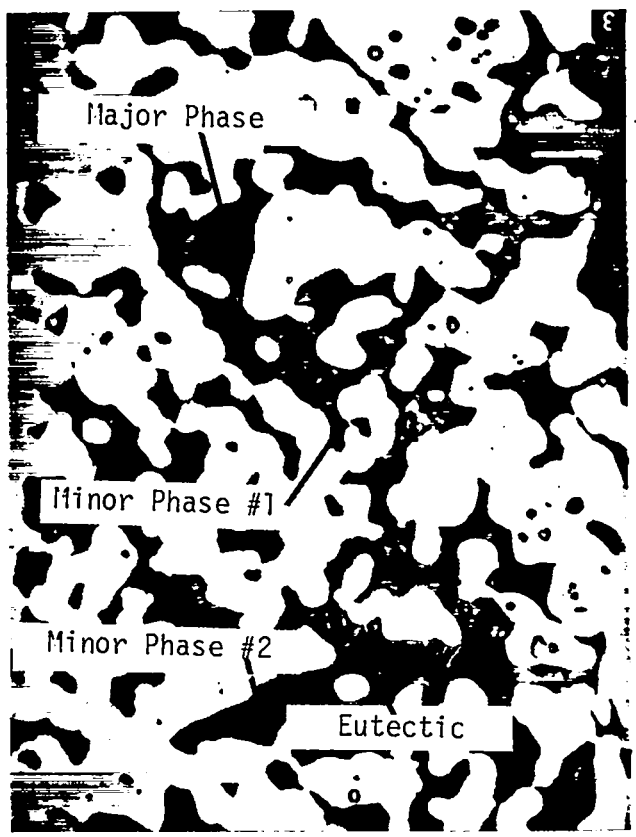

Fig. 19. Nonmetallic deposits in the filter element of the vent assembly of MHW-FSA MHFT-75 (see text for identification). (500X)

Fig. 20. Nonmetallic deposits in the vent hole of MHW-FSA MHFT-75. Both phases contain plutonium and oxygen. (250X)

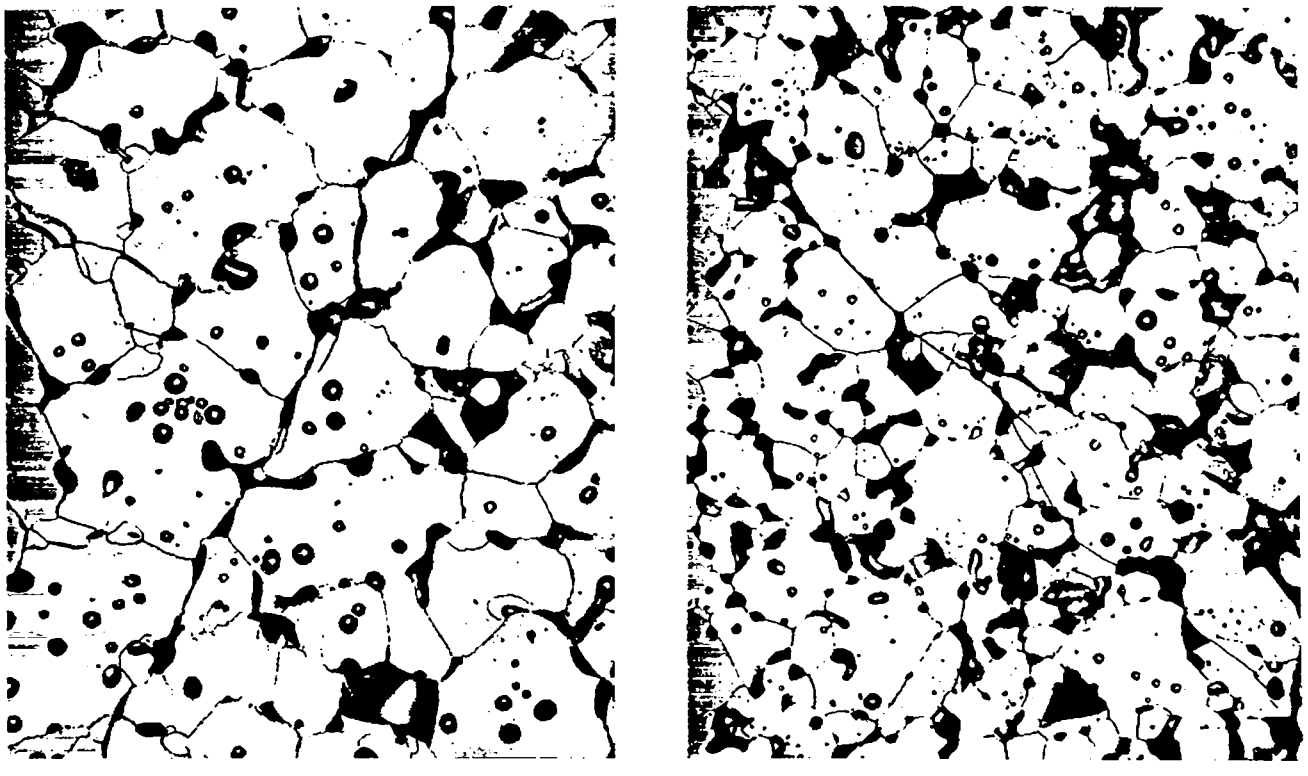

(a) (b)

Fig. 21. Microstructure of the plutonia sphere of MHW-FSA MHFT-75. Note the larger grain size in the surface sample (a) compared to the core sample (b). (both 250X)

TABLE VII. Impact Test Summary of Galileo MHW-FSAs

Assembly Id.	Aging Time (h) 1210°C-GIS Vacuum	ne Impact Test Conditions Reentry T/Impact T Velocity	Postimpact Dimensions Height (mm)	Diam (mm)	% Strain[a] Height/Diam	Failure Type Hoop	Fingerprint[b]	Fuel Push-Through	Other	Iridium Type	Identification
MHFT-61	8834	1550°C/1440°C 74 m/s	31.09	43.46	-23.5/+6.9	No failures				DOP-26	5-1/5-4
MHFT-62	720	1550°C/1440°C 85 m/s	30.38	45.34	-25.6/+12.4	---	---	X	Weld bead Back side	HDR	467-4/468-1
MHFT-64	720	1475°C/1300°C 85 m/s	29.03	45.11	-28.7/+10.8		(X)	---	---	DOP-26	2-1/1-2
MHFT-65	4320	1550°C/1440°C 85 m/s	28.55	43.84	-28.7/+8/0		(X)	X	IF crack extends hoop area	DOP-26	1-1/1-4
MHFT-66	720	1550°C/1440°C 85 m/s	30.68	43.64	-23.8/+6.9	---	X	---	---	HD	462-1/462-4
MHFT-67	100	1500°C/1430°C 74 m/s	29.64	43.66	-27.1/+7.4	No failures				DOP-26	J7-3/J9-2
MHFT-68	110	1792°C/1579°C 82 m/s	30.07	43.66	-27.6/+7.4	No failures				DOP-26	J4-4/J5-2
MHFT-69	100	------/1037°C 82 m/s	30.99	43.71	-23.8/+7.6	---	(X)	---	Weld bead crack-IF	DOP-26	J6-1/J9-4
MHFT-70	720	1500°C/1430°C 82 m/s	29.16	43.26	-28.3/+6.4	---	X	X	---	DOP-26	J4-2/J4-3
MHFT-72	720	1500°C/1430°C 82 m/s	30.43	43.76	-25.1/+7.6	No failures				DOP-26	J22-4/J23-3
MHFT-74	720	1500°C/1430°C 81 m/s	29.74	43.54	-26.8/+7.1	No failures				DOP-26	JR50-1/JR51-2
MHFT-75	720	1500°C/1430°C 81 m/s	30.07	43.23 44.07	-26.0/+6.6-8.3	No failures				DOP-26	L21-5/L22-3

[a] Based upon nominal 40.64 mm diam except MHFT-62 through MHFT-65 based upon MF gaging.

[b] Parentheses indicate penetration confirmed metallographically.

TABLE VIII. Encapsulation of RHU Pellets

	Fuel Pellets[a]			Pt-30Rh Capsules					Welding Box Atmosphere (ppm)		
				No.			Dim. (Welded)[b]				
No.	Diam (in.)	Length (in.)	Weight (g)	Body	Cap	Shim	Diam (in.)	Length (in.)	O_2	H_2O	Capsule Type
RU10-8	0.246	0.371	2.661	122	110	086	0.338	0.498	<1	4	Prime
RU10-11	0.244	0.374	2.668	127	040	146	0.338	0.498	<1	4	Dev.
RU10-12	0.245	0.372	2.646	137	041	147	0.338	0.497	<1	4	Dev.
RU10-13	0.244	0.373	2.662	053	136	104	0.338	0.499	<1	4	Prime
RU10-14	0.245	0.372	2.660	064	137	105	0.337	0.496	<1	4	Prime
RU10-15	0.245	0.372	2.670	074	138	106	0.337	0.495	<1	4	Prime
RU10-16	0.245	0.369	2.668	121	109	085	0.338	0.498	<1	4	Prime
RU9-2	0.245	0.370	2.663	132	111	087	0.338	0.498	<1	4	Prime
RU9-3	0.246	0.366	2.666	133	112	088	0.339	0.496	<1	4	Prime
RU9-4	0.245	0.370	2.665	138	113	089	0.338	0.498	<1	4	Prime
RU9-5	0.246	0.368	2.664	141	114	090	0.338	0.497	<1	4	Prime
RU9-6	0.246	0.370	2.664	142	115	091	0.338	0.497	<1	4	Prime
RU9-7	0.246	0.370	2.667	143	116	094	0.338	0.496	<1	4	Prime
RU9-8	0.246	0.373	2.665	144	117	095	0.338	0.494	<1	4	Prime
RU9-9	0.246	0.366	2.666	146	118	096	0.338	0.498	<1	4	Prime

[a]The specifications for the fuel pellets are diam, 0.245 ± 0.005 in.; length, 0.369 ± 0.007 in.; and weight, 2.664 ± 0.010 g.

[b]Diameters are measured across the machined standoffs, lengths across the welded standoffs. The maximum length that will fit into the graphite shell is 0.504 in.

58 prime units welded last December. The other six prime units and the two developmental units will be used for the Light-Weight Radioisotopic Heater Unit (LWRHU) safety test series. The nondestructive test data obtained to date for these 15 capsules are listed in Table IX.

2. Simulant Units. Ten Pt-30 wt% Rh capsules, seven of them developmental and three prime, were loaded with UO_2 pellets and welded. These units will be used for the LWRHU safety test series. Capsule identification numbers and welded dimensions are listed in Table X.

3. Characterization. To date, we have fabricated 7 lots of LWRHU pellets, 16 pellets per lot. One pellet from each lot was submitted for spectrochemical and isotopic analyses. The spectrochemical data are listed in Table XI and the isotopic data in Table XII.

B. Safety Testing (C. M. Seabourn)

The explosion overpressure thought to be characteristic of a launch-pad explosion of the Space Shuttle is 2000 psi with an impulse of 5.4 psi·s. In preparation for overpressure tests of the heater unit, we have been attempting to reach those values. The pressure was reached easily, but the impulse has proved to be more difficult. So far, the longest impulse we have attained at 2000 psi is 2.7 psi·s.

The test setup has been modified so that the explosion products expand in a spherical chamber before traveling down the cylindrical shock tube. At the reduced pressures used so far, this method does increase the impulse.

IV. SAFETY TECHNOLOGY (D. Peterson, J. Starzynski, and J. Early)

Eight helium release experiments have been completed and analyzed. Los Alamos fuel pellet GP-19, which had been used in a simulated reentry test in October 1980, was broken, and the fragments were exposed to temperature ramps up to 1600°C, with heating rates ranging from 10 to 580°C/min. The dynamic helium release data measured were analyzed assuming classical diffusion laws.

The results of the analyses of the eight runs are shown in Table XIII. The heating rate given each sample is shown in the first column. The activation energy E_a and the effective diffusion constant D'_0 are listed next. The logarithm of the diffusion constant D′ is plotted versus

TABLE IX. NDT for Encapsulated RHU Pellets

Fuel Pellet No.	Weight (g)	Capsule Body No.	α Swipe (counts/min)[a]	Helium Leak Rate (cm^3/s)	Neutron Emission Rate (n/s-g ^{238}Pu)	Comments
RU10-8	2.661	122	0	5.1×10^{-10}	4 868	
RU10-11	2.668	127	0	5.7×10^{-10}	4 278	Dev. capsule for test
RU10-12	2.646	137	0	5.7×10^{-10}	4 376	Dev. capsule for test
RU10-13	2.662	053	0	5.7×10^{-10}	4 305	
RU10-14	2.660	064	0	5.7×10^{-10}	4 487	
RU10-15	2.670	074	0	5.7×10^{-10}	4 534	
RU10-16	2.668	121	0	5.1×10^{-10}	4 547	
RU9-2	2.663	132	0	5.1×10^{-10}		
RU9-3	2.666	133	0	5.1×10^{-10}		
RU9-4	2.665	138	0	5.1×10^{-10}		
RU9-5	2.664	141	0	3.5×10^{-10}		
RU9-6	2.664	142	0	3.5×10^{-10}		
RU9-7	2.667	143	0	3.5×10^{-10}		
RU9-8	2.665	144	0	3.5×10^{-10}		
RU9-9	2.666	146	0	3.5×10^{-10}	4 919	

[a]The specifications are α swipe = <220 counts/min; helium leak rate = $<1 \times 10^{-6}$ cm^3/s; neutron emission rate = <6 000 n/s-g ^{238}Pu; and calorimetry = 1.10 ± 0.03 W.

TABLE X. Encapsulation of Simulant RHU Pellets

Pt-30Rh Capsule Body	Cap	Shim	Welded Dimensions[a] Diam (in.)	Length (in.)	Capsule Type[b]
011	023	093	0.338	0.500	Dev.
030	028	134	0.338	0.503	Dev.
038	029	135	0.337	0.503	Dev.
044	030	136	0.338	0.497	Dev.
072	032	138	0.338	0.496	Dev.
124	037	143	0.338	0.495	Dev.
125	038	144	0.338	0.497	Dev.
087	106	082	0.338	0.497	Prime
119	107	083	0.338	0.501	Prime
120	108	084	0.338	0.495	Prime

[a]Diameters are measured across the machined standoffs, lengths across the weld standoffs. The maximum allowed length is 0.504 in.

[b]Each capsule contains a UO_2 pellet.

the reciprocal temperature in Fig. 22. Since points were taken every 6 s, individual data values are not plotted, but rather the least-squares line for each ramp is shown. There appears to be a general trend towards lower activation energies and effective diffusion coefficients as the heating rate is decreased. The reproducibility appears to be good except in Run 5 at 145°C/min. Runs 13 and 11 at 580°/min give essentially the same D′, E_a, and D'_o values. Runs 9 and 10 give about the same D′ value, although Run 10 has a higher E_a value. These differences may arise in part from variances in the microstructure, since the samples were randomly selected without regard to the region of the pellet. The role of the grain boundaries in determining the release rate is being examined experimentally as well as theoretically.

REFERENCES

1. S. E. Bronsiz, Compiler, "Space Nuclear Safety and Fuels Program, April 1981," Los Alamos National Laboratory report LA-8968-PR (July 1981).
2. T. L. Markin and M. H. Rand, "Thermodynamics," Vol. 1, *Proc. Symp. Thermodyn. Nuc. Mater. At.*

TABLE XI. Spectrochemical Data for RHU Pellet Lots (ppm by weight)

Species	Limit[a]	Sensitivity Limit	LWRHU Pellet Lots RU3	RU4	RU5	RU6	RU7	RU9	RU10	Av
Al	150	5	250	50	30	35	360	290	15	147
B	1	1	5	<	2	1	<	<	<	1
Ca	300	3	10	10	8	50	130	50	50	44
Cd	50	10	<[b]	<	<	<	<	<	<	<
Cr	250	5	45	220	260	130	140	85	85	138
Cu	100	1	5	1	<	<	2	<	<	1
Fe	800	5	280	430	390	190	290	160	180	274
Mn	50	1	15	5	4	7	4	5	10	7
Mo	50	3	3	4	4	4	<	4	<	3
Na	250	2	2	3	2	4	<	4	10	8
Ni	150	5	30	20	30	15	35	6	20	22
Pb	100	5	5	<	<	<	<	<	<	1
Si	200	5	290	180	150	150	230	140	220	194
Sn	50	5	7	5	5	5	<	<	<	3
Zn	50	5	10	20	10	15	10	15	20	14

[a]The specifications are 800 ppm for iron and 200 ppm for silicon. All other elements listed are to be reported.
[b]Less than sensitivity limit, not detected in sample.

TABLE XII. Isotopic Data for RHU Pellets (wt %)

Pu Isotope	Feed Material[a] Sr Calc.	Los Alamos Meas.	LWRHU Pellet Lots RU3	RU4	RU5	RU6	RU7	RU9	RU10	Av
238	83.39	83.34	83.34	83.42	83.38	83.45	83.37	83.33	83.36	83.38 ± 0.04
239	14.07	14.11	14.12	14.05	14.08	14.08	14.09	14.12	14.10	14.09 ± 0.02
240	1.99	1.99	1.99	1.99	1.99	1.95	1.99	2.00	1.99	1.99 ± 0.02
241	0.42	0.42	0.43	0.42	0.42	0.37	0.42	0.43	0.42	0.42 ± 0.02
242	0.12	0.13	0.13	0.13	0.13	0.15	0.13	0.13	0.13	0.13 ± 0.01

[a]All values were corrected for decay from the date of measurement to July 1, 1981.

TABLE XIII. Results of Helium Release Measurements on Samples of Pellet GP-19

Run No.	Heating Rate (°C/min)	E_a (kcal)	$\log_{10} D_o' s^{-1}$
3	10	49.7	2.39
5	145	86.8	4.70
8	58	71.3	4.79
9	145	70.8	4.55
10	145	88.5	6.86
11	580	126.0	11.30
12	580	118.1	9.55
13	580	121.7	10.85

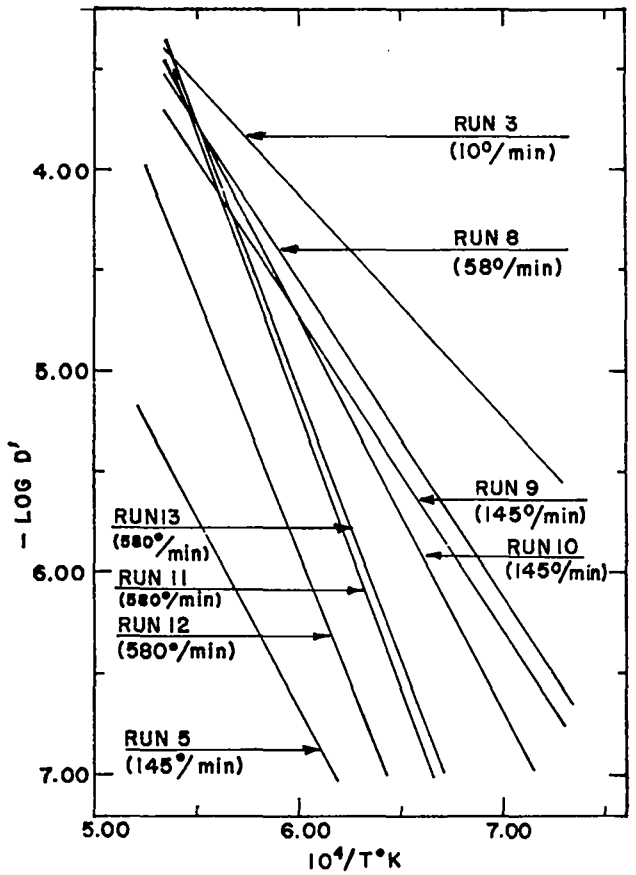

Fig. 22. Diffusion constant D' versus reciprocal temperature for various temperature ramps.

Transp. Solids, 1965, (International Atomic Energy Agency, Vienna, 1966), p. 145.

3. R. J. Ackerman, R. L. Faircloth, and M. H. Rand, "A Thermodynamic Study of the Vaporization Behavior of the Substoichiometric Plutonium Dioxide Phase," J. Phys. Chem. 70, No. 11, 3698-3706 (1966).

Additional Distribution

B. J. Rock, Dept. of Energy/SNS, Washington, DC
G. L. Bennett, Dept. of Energy/SNS, Washington, DC
J. J. Lombardo, Dept. of Energy/SNS, Washington, DC
R. B. Morrow, Dept. of Energy/SNS, Washington, DC
C. O. Tarr, Dept. of Energy/SNS, Washington, DC
R. Brouns, Dept. of Energy/SNS, Washington, DC
J. Griffo, Dept. of Energy/SNS, Washington, DC
R. Ferguson, Dept. of Energy/ET, Washington, DC
D. K. Stevens, Dept. of Energy/BES, Washington, DC
R. L. Clark, Dept. of Energy/ALO, Albuquerque, NM
H. N Hill, Dept. of Energy/DAO, Miamisburg, OH
M. J. Sires, Dept. of Energy/SRO, Aiken, SC
R. J. Hart, Dept. of Energy/ORO, Oak Ridge, TN
W. L. Von Flue, Dept. of Energy, SFOO, Oakland, CA
T. B. Kerr, NASA Washington, DC
R. A. Ivanoff, NASA/JPL, Pasadena, CA
G. Stapfer, NASA/JPL, Pasadena, CA
R. Campbell, NASA/JPL, Pasadena, CA
AFISC/SNS, Attn: Col. J. A. Richardson, KAFB, Albuquerque, NM
AFWL/NTYVS, Attn: Capt. J. D. Martens, KAFB, Albuquerque, NM
HQ Space Div./YLVS, Attn: Lt. Col. Needham, Los Angeles, CA
R. L. Folger, SRL, Aiken, SC
J. Howell, SRL, Aiken, SC
J. B. Mellen, SRP, Aiken, SC
G. W. Wilds, SRP, Aiken, SC
D. Nichols, SRP, Aiken, SC
J. R. McClain, MRC, Miamisburg, OH
W. T. Cave, MRC, Miamisburg, OH
W. Amos, MRC, Miamisburg, OH
E. W. Johnson, MRC, Miamisburg, OH
H. Postma, ORNL, Oak Ridge, TN
R. Cooper, ORNL, Oak Ridge, TN
H Inouye, ORNL, Oak Ridge, TN
E. Foster, BCL, Columbus, OH
C. Alexander, BCL, Columbus, OH
J. Hagan, APL, Baltimoe, MD
R. W. Englehart, NUS Corp., Rockville, MD
H. H. Van Tuyl, PNL, Richland, WA
A. Shock, Fairchild-Hiller Ind., Germantown, MD
C. W. Whitmore, GE, Philadelphia, PA
R. Hemler, GE, Philadelphia, PA
V. Haley, GE, Philadelphia, PA
E. C. Krueger, Sundstrand, Rockford, IL
F. Schumann, TES, Timonium, MD
J. Boretz, TRW, Redondo Beach, CA
R. Hartman, GE, Philadelphia, PA
W. Mecham, ANL, Argonne, IL
J. Birely, Los Alamos, NM
W. J. Maraman, Los Alamos, NM
S. S. Hecker, Los Alamos, NM
R. N. R. Mulford, Los Alamos, NM
W. F. Miller, Los Alamos, NM
R. J. Pryor, Los Alamos, NM
G. R. Waterbury, Los Alamos, NM
R. Behrens, Los Alamos, NM

S. E. Bronisz, Los Alamos, NM
R. A. Kent, Los Alamos, NM
W. Stark, Los Alamos, NM
R. W. Zocher, Los Alamos, NM
J. A. Pattillo, Los Alamos, NM

Printed in the United States of America
Available from
National Technical Information Service
US Department of Commerce
5285 Port Royal Road
Springfield, VA 22161
Microfiche $3.50 (001)

Page Range	Domestic Price	NTIS Price Code	Page Range	Domestic Price	NTIS Price Code	Page Range	Domestic Price	NTIS Price Code	Page Range	Domestic Price	NTIS Price Code
001-025	$ 5.00	A02	151-175	$11.00	A08	301-325	$17.00	A14	451-475	$23.00	A20
026-050	6.00	A03	176-200	12.00	A09	326-350	18.00	A15	476-500	24.00	A21
051-075	7.00	A04	201-225	13.00	A10	351-375	19.00	A16	501-525	25.00	A22
076-100	8.00	A05	226-250	14.00	A11	376-400	20.00	A17	526-550	26.00	A23
101-125	9.00	A06	251-275	15.00	A12	401-425	21.00	A18	551-575	27.00	A24
126-150	10.00	A07	276-300	16.00	A13	426-450	22.00	A19	576-600	28.00	A25
									601-up	†	A99

† Add $1.00 for each additional 25-page increment or portion thereof from 601 pages up

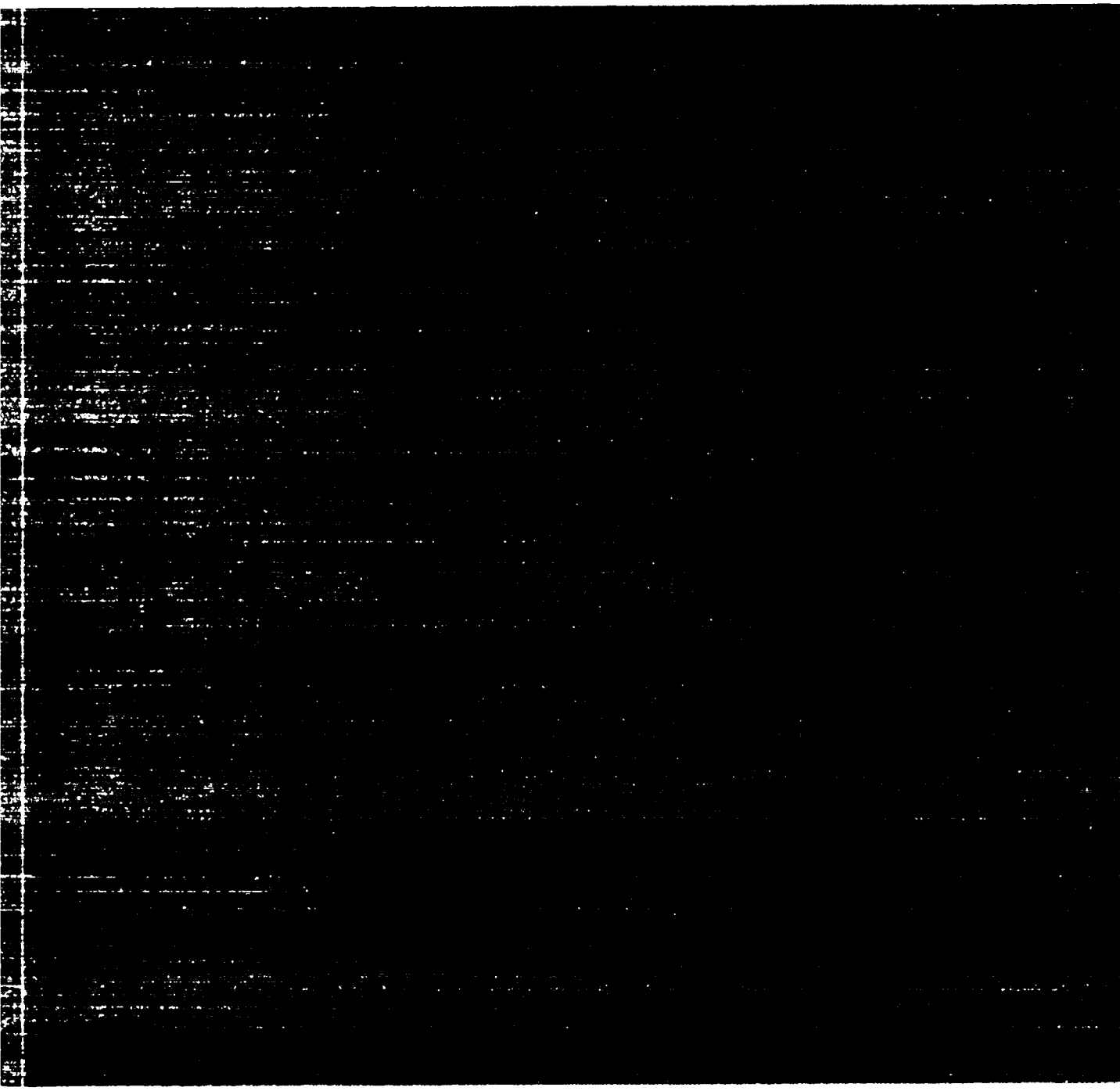

Los Alamos